RESEARCH ARTICLE

Editorial Process: Submission:11/07/2025 Acceptance:07/13/2026 Published:07/27/2026

Isorhamnetin-3-O-Neohesperidoside Exerts Anti-Hepatocellular Carcinoma Activity by Targeting Multiple Oncogenic Pathways

Flavian Borgia Sherin Rebecca[1]*, Ramanathan Sharmila[1], Rajamanickam Pon Nivedha[2]

Abstract

Background: The objective of this study was to investigate the inhibitory effects and underlying molecular mechanisms of Isorhamnetin-3-O-neohesperidoside (IHN), a naturally occurring O-methylated flavonol, against human hepatocellular carcinoma (HepG2) cells, with a particular focus on its impact on cell proliferation, apoptosis, metabolic regulation, and oxidative stress. **Methods:** Human liver cancer HepG2 cells were treated with varying concentrations of IHN for 24 and 48 hours. The cytotoxic and anti-proliferative effects were assessed using standard cytotoxicity assays. Flow cytometry was performed to analyze cell cycle distribution and apoptosis induction. Metabolic assays evaluated glucose uptake and lactate dehydrogenase A (LDH-A) activity to assess the Warburg effect. Oxidative stress markers were analyzed by measuring reactive oxygen species (ROS), lipid peroxidation, and the glutathione (GSH/GSSG) ratio. Quantitative real-time PCR (qRT-PCR) was used to determine the expression of key regulatory genes. **Results:** IHN exhibited potent, dose- and time-dependent cytotoxicity against HepG2 cells, with Half-maximal inhibitory concentration (IC_{50}) values decreasing from 161.22 μM (24 h) to 95.87 μM (48 h). IHN- induced G0/G1 cell cycle arrest accompanied by the upregulation of Cyclin-dependent kinase inhibitor 1A (CDKN1A/p21) and promoted apoptosis through the intrinsic pathway, as shown by increased expression of BCL2-associated X Protein (BAX), Caspase-3 (CASP-3), and Caspase-9 (CASP-9). Metabolically, IHN suppressed the Warburg effect, leading to reduced glucose uptake and decreased LDH-A activity. This was associated with a marked increase in ROS levels and lipid peroxidation, along with depletion of GSH/GSSG and downregulation of antioxidant genes, indicating severe oxidative stress. **Conclusion:** IHN exerts significant anti-hepatocellular carcinoma activity by targeting multiple oncogenic pathways. Its mechanism involves cell cycle arrest, intrinsic apoptosis induction, metabolic suppression, and redox imbalance. These findings suggest that IHN is a promising multi-target natural compound that exploits the metabolic and oxidative vulnerabilities of HepG2 cells, highlighting its potential as a novel therapeutic candidate for hepatocellular carcinoma.

Keywords: isorhamnetin- liver cancer- cancer therapy- gene expression- molecular signaling

Asian Pac J Cancer Prev, **27 (7)**, 2589-2599

Introduction

Hepatocellular Carcinoma (HCC) represents the vast majority (90%) of primary liver cancers and contributes significantly to the disease's status as the fourth deadliest cancer globally (over 800,000 deaths/year). Importantly, most HCC cases are preventable, as they are associated with recognizable causes, including chronic viral hepatitis, excessive alcohol use, and non-alcoholic fatty liver disease [1]. Currently, immunotherapies, systemic medications, loco-regional treatments, surgery, and transplantation are all used in treatment. Although transplants and surgery may be curative, systemic and combination therapies are necessary for the majority of severe cases. Multidisciplinary novel approaches are necessary in view of ongoing adverse effects and other limitation factors [2]. Medicinal plants with varied phytochemicals, including terpenoids, alkaloids, flavonoids, and phenolics, have made them well known for their medicinal potential against a wide range of illnesses. Due to their anti-inflammatory, anti-oxidant, antibacterial, and immunomodulatory properties, these substances are useful in the treatment of cancer, diabetes, heart disease, and neurological disorders. Relatively, contemporary medications, such as antimalarials like artemisinin and anticancer treatments like paclitaxel, are derived from plants and their effectiveness in current treatment methods shows the significance in drug development

*[1]PG and Research Department of Biotechnology, Bishop Heber College (Autonomous), Bharathidasan University, Tiruchirappalli, Tamil Nadu, India. [2]PG and Research Department of Biotechnology and Bioinformatics, Holy Cross College (Autonomous), Tamil Nadu, India. *For Correspondence: sherinborgia@gmail.com*

[3]. Isorhamnetin is a naturally occurring O-methylated flavonol, a flavonoid compound obtained from herbal medicinal plants including berries, Oenanthe javanica, and Ginkgo biloba. It has a broad range of pharmacological properties, including as neuroprotective, cardioprotective, anti-inflammatory, anticancer, and antioxidant actions [4, 5]. Moreover, recently studies have reported its anticancer effects against various types of cancer, including esophageal [6] and gastric cancer [7] leukemia [8], skin [9] colon [10] cancers. Though the inhibitory effects of isorhamnetin on liver cancer has been discussed shortly, the deep molecular mechanisms underlying its effects remain unclear [11]. Molecular pathway targeting is essential for drug development, including the application of medicinal plants. Natural substances have the ability to alter cellular signaling pathways, which makes them possible adjuvants in cancer treatment also certain pathways like, PhosphatidylInositol 3-Kinase/ Protein Kinase B (PI3K/Akt) and Rat Sarcoma/Mitogen-Activated Protein Kinase (Ras/MAPK) are frequently reported to be dysregulated in cancerous condition. Numerous natural substances have shown anticancer action against a variety of cancer types, and understanding their signalling routes is crucial [12]. For instance, studies reported Isorhamnetin exerts anticancer effects by modulating multiple cellular signaling pathways and induces ROS-dependent apoptosis in breast cancer cells. Notably, it shows higher cytotoxicity at lower doses than quercetin in various cancer cells, including breast and leukemia [13]. Therefore, to find possible treatment targets, a comprehensive understanding of the alterations in cell signaling pathways is necessary. In this study, the inhibitory effect of isorhamnetin and the proliferation of several liver cancer cell lines were investigated, along with the cell signaling pathways involved in its pharmacological actions, that gives a better understanding about the mechanism behind isorhamnetin's effects on liver cancer.

Materials and Methods

Cell culture

Human liver cancer cell line, HepG2 were obtained from National Centre for Cell Science (NCCS), Pune. Passaging and maintenance of the cells were carried out in a CO2 incubator, supplemented with 10% fetal bovine serum (FBS), a combination of 1% penicillin and streptomycin antibiotics, and Dulbecco's Modified eagle Medium (DMEM) media, HiMedia.

Cell viability assay

To assess the cytotoxic potential of IHN against liver cancer, HepG2 cells were cultured and exposed to varying concentrations of the compound ranging from 0 to 250 µM for 24 and 48 hours. Two complementary assays were employed to evaluate cell viability: the (3-[4,5-dimethylthiazol-2-yl]-2,5-diphenyl tetrazolium bromide) (MTT) assay and the Trypan Blue exclusion assay. For the MTT assay, cells were seeded into 96-well plates at a density of approximately 1×10^4 cells/well and allowed to adhere overnight. After treatment with the compound for the indicated time points, 20 µL of MTT reagent (5 mg/mL) was added to each well and incubated at 37°C for 4 hours. The resulting formazan crystals were solubilized in DMSO (dimethyl sulfoxide), and absorbance was measured at 570 nm using a microplate reader. The percentage of viable cells was calculated relative to untreated control wells. The Trypan Blue exclusion assay was conducted to determine membrane integrity and further validate cytotoxic effects. Treated and control HepG2 cells were harvested, stained with 0.4% Trypan Blue solution, and counted using a hemocytometer. The number of viable (unstained) and dead (blue-stained) cells was recorded, and viability was expressed as a percentage of total cells [14].

IHN treatment

HepG2 cells were seeded and allowed to reach appropriate confluency prior to treatment. For cytotoxicity assessment, cells were treated with IHN at concentrations ranging from 0 to 250 µM for 24 and 48 hours to determine dose- and time-dependent effects and calculate IC_{50} values. Based on the IC_{50} values obtained (161.22 µM at 24 h and 95.87 µM at 48 h), an IC_{50}-based sublethal concentration (~100 µM) was selected for all subsequent mechanistic experiments, including immunofluorescence staining, flow cytometric analysis of cell cycle and apoptosis, glucose uptake and LDH-A assays, oxidative stress measurements [ROS, Malondialdehyde (MDA)], glutathione analysis, and qRT-PCR studies.

Immunofluorescence assays

HepG2 cells were cultured in DMEM supplemented with 10% fetal bovine serum (FBS), 1% penicillin-streptomycin, and maintained at 37°C in a humidified atmosphere containing 5% CO_2. Upon reaching approximately 70–80% confluency, the cells were treated with an optimized concentration of IHN for 24 hours and 48 hours, while untreated cells served as the control group. To evaluate morphological alterations, live cells were observed under a brightfield microscope using a 20× objective lens. Images were captured on an Olympus inverted microscope to document changes in cellular morphology and confluency post-treatment. Intracellular ROS generation was assessed using 2′,7′-dichlorofluorescein diacetate (DCF-DA) staining. After treatment, cells were washed with PBS and incubated with 10 µM DCF-DA in serum-free media at 37°C for 30 minutes in the dark. Following incubation, cells were washed and visualized under a fluorescence microscope (excitation 488 nm/emission 525 nm). ROS-positive cells exhibited green fluorescence intensity proportional to ROS levels. To detect apoptotic and necrotic changes, Acridine Orange (AO) and Ethidium Bromide (EtBr) dual staining was performed. Treated and control cells were washed with PBS and stained with a 1:1 mixture of AO (100 µg/mL) and EtBr (100 µg/mL) for 5 minutes in the dark. Stained cells were immediately examined under a fluorescence microscope. AO permeates all cells and stains the nuclei green, whereas EtBr penetrates only membrane-compromised cells, staining their nuclei orange-red. Thus, viable cells appear green, early apoptotic cells appear bright green with condensed nuclei, and late apoptotic/ necrotic cells appear orange/red were observed under

Olympus microscope (#BX53, Tokyo, Japan), equipped with a Zenoptik camera [15].

Flow cytometry analysis

Flow cytometric analysis was utilized to investigate the DNA content across different phases of the cell cycle. HepG2 cells were seeded and treated with IHN for 24 and 48 hours, following a 24-hour incubation period. After the treatment, the cells were fixed overnight in 70% ice-cold ethanol. Subsequently, the fixed cells were stained with propidium iodide (PI) dye after treatment with RNase A at a concentration of 10 mg/mL. The fluorescence emitted by the PI-labeled nuclei was then quantified using a flow cytometer. To evaluate the apoptotic cells, an Annexin V-FITC Apoptosis Kit was employed according to the manufacturer's instructions. Following 48 hours of treatment with IHN, the cells were stained with PI and Annexin V-FITC for 15 minutes at 25°C in the dark. The apoptotic index was analyzed using flow cytometry with a BD FACS Calibur instrument, and the data interpretation was conducted using Cell Quest Pro version 3.2.1 (Becton Dickinson, USA) [16].

Glucose uptake and Lactate dehydrogenase assay

HepG2 cells were seeded at a density of 1×10^5 cells/well in 6-well culture plates and allowed to adhere overnight. Subsequently, the cells were treated with IHN at an optimized dose for 24 hours and 48 hours, while untreated cells served as controls. Glucose uptake in HepG2 cells was quantified using a commercially available 2-Deoxyglucose (2DG) ELISA kit following the manufacturer's protocol. Briefly, after treatment, cells were washed with PBS and lysed using the lysis buffer provided in the kit. The cell lysates were collected and centrifuged at 12,000 × g for 10 minutes at 4°C to remove debris. Supernatants were transferred to a 96-well microplate coated with a 2DG capture antibody. The assay was performed by adding standards and samples into the wells, followed by incubation with biotinylated detection antibodies, HRP-conjugated streptavidin, and TMB substrate solution. The reaction was stopped with sulfuric acid, and absorbance was measured at 450 nm using a microplate reader. The amount of 2DG uptake was quantified against a standard curve and expressed as pmol/µg protein [17].

LDH-A enzyme activity was determined using an LDH-A specific ELISA kit according to the manufacturer's instructions. After treatment, HepG2 cells were harvested, washed, and lysed in the supplied assay buffer. After centrifugation, 100 µL of supernatant was added to the microplate wells pre-coated with LDH-A capture antibodies. The samples were incubated with detection antibodies and enzyme conjugates sequentially, followed by the chromogenic substrate. The colorimetric reaction was stopped, and absorbance was measured at 450 nm. The LDH-A activity was calculated based on a standard curve and expressed as arbitrary units (AU) per µg protein [17].

Measurement of Intracellular ROS Levels

For experimental treatments, HepG2 cells were seeded at a density of 1×10^5 cells/well in 6-well plates. After 24 hours of incubation, cells were treated with IHN for 24 and 48 hours, while untreated cells served as negative controls. Intracellular ROS levels were determined using a cell-based ROS detection ELISA kit, following the manufacturer's instructions. After treatment, cells were washed with Phosphate Buffer Saline (PBS), lysed using the provided lysis buffer, and the lysates were collected by centrifugation at 12,000 × g for 10 minutes at 4°C. The supernatant was transferred to ELISA plate wells pre-coated with ROS detection antibodies. Samples and standards were added, followed by incubation with biotin-labeled anti-ROS antibodies and HRP-conjugated streptavidin. The enzymatic reaction was developed using TMB substrate and stopped with sulfuric acid. Absorbance was measured at 450 nm using a microplate reader. ROS levels were quantified against a standard curve and expressed as arbitrary units (AU) per µg of total protein [17].

Quantification of Lipid Peroxidation by MDA levels

To assess LPO, MDA levels were measured using a competitive ELISA kit specific for malondialdehyde. Following treatment, cell lysates were prepared using the supplied lysis buffer and centrifuged to remove debris. Equal volumes of the supernatant were incubated with biotin-labeled MDA standards or samples in the pre-coated ELISA plates. HRP-conjugated secondary antibody was added, followed by TMB substrate for color development. The reaction was stopped, and absorbance was measured at 450 nm. MDA levels were calculated using a standard curve and expressed as nanomoles (nmol) per mg protein [17].

Measurement of GSH Levels

HepG2 cells were seeded at a density of 1×10^6 cells per well in 6-well plates and allowed to adhere overnight. The cells were then treated with IHN for 24 hours and 48 hours. Untreated cells served as the control group. The intracellular levels of GSH were quantified using a commercially available GSH ELISA kit according to the manufacturer's protocol. Post-treatment, the cells were harvested, washed twice with cold PBS, and lysed using the lysis buffer provided in the kit. The lysates were then centrifuged at 12,000 × g for 10 minutes at 4°C to remove cell debris. The supernatants were collected and added to ELISA plates pre-coated with GSH-specific antibodies. The assay involves derivatization of GSH followed by enzymatic recycling involving glutathione reductase, where the rate of the colorimetric reaction is proportional to the GSH concentration. The absorbance was read at 450 nm using a microplate reader. A standard curve was generated using known concentrations of GSH, and sample concentrations were calculated accordingly and expressed as nmol GSH per 10^6 cells [17].

Measurement of GSH/GSSG Ratio

The GSH/GSSG ratio was determined using a GSH/GSSG quantification ELISA kit. Following IHN treatment, cells were harvested and lysed. For accurate detection of GSSG, total glutathione was first derivatized to mask

reduced GSH, allowing selective measurement of GSSG. The GSSG content was then determined, and total GSH was measured in parallel samples without derivatization. The GSH/GSSG ratio was calculated by dividing the total GSH by the GSSG value in each sample. Samples and standards were added to microplate wells along with HRP-conjugated secondary antibody and incubated. Color development was achieved using TMB substrate, and the reaction was stopped with a sulfuric acid stop solution. The absorbance was read at 450 nm. Data were calculated against a standard curve and reported as GSH/GSSG ratio values [17].

Gene expression by RT-PCR

HepG2 cells were seeded around 5×10^6 cells per well in a 6-well plate. Then, RNA extraction was carried out using TRIR from Abgene, UK. The concentration of the extracted RNA was determined through spectrometric quantification, measured in micrograms (µg). For mRNA expression by Real-Time PCR, a reaction mixture was meticulously prepared using Takara SyBr green master mix with custom-designed forward and reverse primers targeting genes and the thermal cycling consisted of an initial activation step lasting 5 minutes at 95°C, followed by 40 cycles of a two-step cycling process. This cycling involves denaturation for 5 seconds at 95°C, followed by combined annealing and extension for 10 seconds at the specific primer temperature, which ranges between 55°C and 62.5°C. The RT-PCR was quantified and equipped with CFX9 real touch bio-rad system, USA [14]. The primer sequences used in this study are provided in the Table.1. Inflammatory mediators [Nuclear factor kappa B (NF κB), Tumor necrosis factor-alpha TNF α)] were included to evaluate whether IHN modulates tumor-promoting inflammatory signaling, given the established role of inflammation in cancer cell survival, proliferation, and apoptosis.

Statistical analysis

Data are presented as mean ± standard deviation (SD) from three independent experiments (n = 3). Data distribution was assessed prior to statistical testing, and all datasets followed approximate normal distribution; therefore, parametric tests were applied. Comparisons between two groups were performed using a two-tailed Student's t-test, while comparisons among multiple groups were conducted using one-way analysis of variance (ANOVA). A p value of <0.05 was considered statistically significant. Additional significance levels ($p<0.001$ and $p<0.0001$) are reported to denote increasing strength of statistical evidence against the null hypothesis and do not represent different decision criteria. For outcome measures, 95% confidence intervals (CI) were calculated to indicate the precision and reliability of the estimated effects. Statistical analysis was performed using GraphPad Prism 8.

Results

Cytotoxicity study

The MTT assay revealed a dose- and time-dependent decrease in cell viability following treatment with IHN. As shown in the Figure 1, a progressive decline in viability was observed with increasing concentrations of the compound at both 24 and 48 hours. Notably, IC_{50} values were 161.22 µM at 24 h and 95.87 µM at 48 h, with 95% confidence intervals indicating a narrow and reliable estimation of cytotoxic potency. These results suggest

Table 1. RT-PCR Primers Used in This Study

S. no	Gene name	Primers (5 ′---------- 3 ′)	Reference
1	*BAX*	F-TTCTGACGGCAACTTCAACTG	[18]
		R-TGAGGAGTCTCACCCAACCA	
2	*CASP3*	F- CTTCAGTGGTGGACATGACG	[19]
		R- TCAACAATTTGAGGCTGCTG	
3	*CASP9*	F- AGCCAGATGCTGTCCCATAC	[19]
		R- CAGGAACCGCTCTTCTTGTC	
4	*P53*	F- AGCCAGATGCTGTCCCATAC	[18]
		R- CAGGAACCGCTCTTCTTGTC	
5	*BCL2*	F-GACGCTTTGCCACGGTGGTG	[18]
		R-GGGGCAGGCATGTTGACTTCAC	
6	*Survivin*	F-ACCGCATCTCTACATTCAAG	[20]
		R-CAAGTCTGGCTCGTTCTC	
7	*BCL-XL*	F-GTAAACTGGGGTCGCATTGT	[21]
		R-TGCTGCATTGTTCCCATAGA	
8	*BAD*	F-CCCAGAGTTTGAGCCGAGTG	[22]
		R-CCCATCCCTTCGTCGTCCT	
9	*CCND1*	F- GAGACCATCCCCCTGACGGC	[23]
		R- TGACGGGGTCACCCACACT	
10	*CDK4*	F-TGCCAATTGCATCGTTCACCGAG	[24]
		R- TGCCCAACTGGTCGGCTTCA	
11	*CDKN1A*	F- TGTCCGTCAGAACCCATGC	[23]
		R- AAAGTCGAAGTTCCATCGCTC	
12	*P27*	F- TGGAGAAGCACTGCAGAGAC	[25]
		R-GCGTGTCCTCAGAGTTAGCC	
13	*SOD1*	F- GTCTGGCCTATAAAGTAGTCG	[26]
		R- AGCGGCCTCGCAACACAA	
14	*CAT*	F-ATCTGCTTCATCGCCTACTT	[27]
		R-TCTCTGCCTCTGGTAAAAAC	
15	*NRF2*	F- ACACGGTCCACAGCTCATC	[28]
		R- TGCCTCCAAGTATGTCAATA	
16	*HO1*	F-GTC CAA CAT CCA GCT CTT TGA GG	[29]
		R-GAC AAA GTT CAT GGC CCT GGG A	
17	*NF-κβ*	F- ATGCATGCTAGCTAGCTAGC	[30]
		R- GCTAGCTAGCTAGCATGCAT	
18	*TNF-α*	F- ACAAGCCTGTAGCCCATGTT	[30]
		R- AAAGTAGACCTGCCCAGACT	
19	*IL-6*	F-TCAATGAGGAGACTTGCCTG	[30]
		R- GATGAGTTGTCATGTCCTGC	
20	*C-MYC*	F- TCAAGAGGCGAACACACAAC	[31]
		R- GGCCTTTTCATTGTTTTCCA	
21	*β-Actin*	F-AACAAGATGAGATTGGCA	[18]
		R-AGTGGGGTGGCTTTTAGGAT	

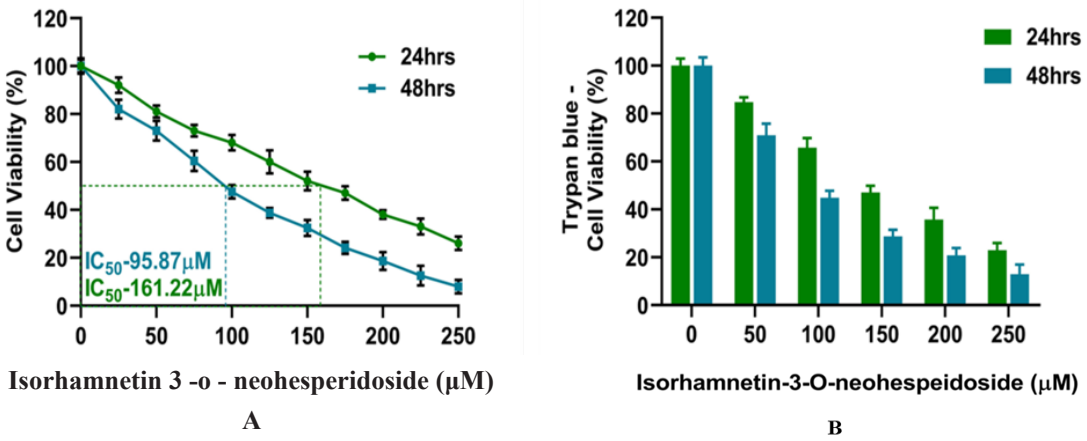

Figure 1. Cytotoxic Effects of IHN on HepG2 Cells. Data are presented as mean ± SD (n = 3); 95% confidence intervals were calculated for outcome measures.

that IHN significantly suppresses HepG2 cell metabolic activity in a time-dependent manner. Complementary findings were obtained from the Trypan Blue exclusion assay, as illustrated in the right panel. This method confirmed a concentration-dependent decline in viable cell count, with a more pronounced effect at 48 hours. At higher concentrations (≥150 µM), cell viability dropped below 40%, particularly after 48 hours of treatment. This confirms a substantial loss of membrane integrity, consistent with advanced stages of cytotoxic damage. The findings from both viability assays collectively underscore the potent anti-proliferative activity of IHN against HepG2 liver cancer cells. The observed time- and dose-dependent cytotoxicity reflects the compound's potential to induce cellular stress and inhibit survival mechanisms in malignant hepatocytes.

(A) Cell viability after 24 and 48 h treatment (0–250 µM), showing a dose- and time-dependent decline with IC_{50} values of 161.22 µM (24 h) and 95.87 µM (48 h). (B) Trypan Blue exclusion assay confirming reduced viable cell counts, with viability dropping below 40% at ≥150 µM, particularly after 48 h, indicating loss of membrane integrity and advanced cytotoxic damage.

Immunofluorescence staining

As shown in Figure 2, control HepG2 cells maintained healthy, spindle-like morphology with high confluency, while IHN treatment caused a time-dependent reduction

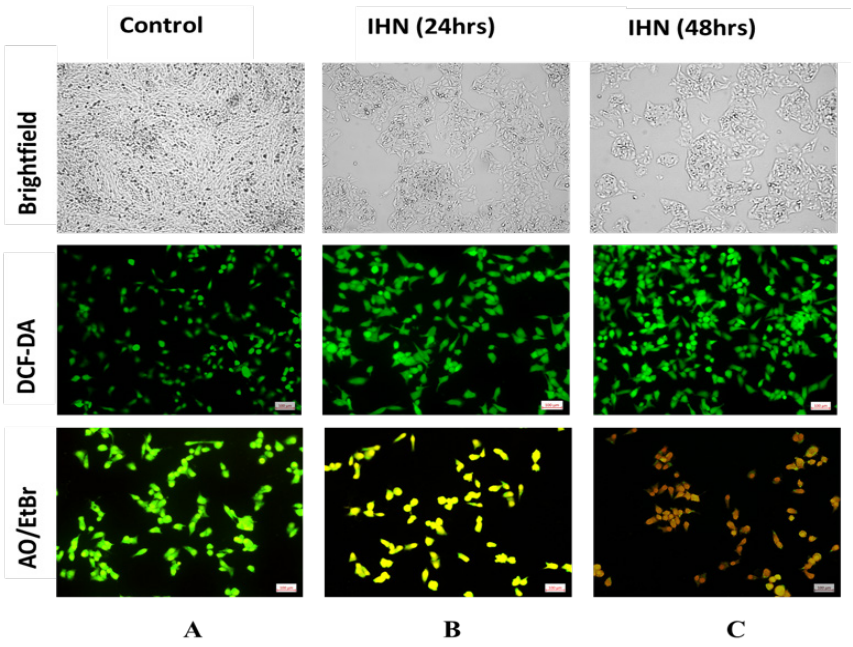

Figure 2. Morphological and Biochemical Assessment of Apoptosis and Oxidative Stress in HepG2 Cells Following IHN Treatment. The figure shows representative images of HepG2 cells under three experimental conditions: (A) Control (untreated cells), (B) IHN-treated cells (24 hours), and (C) IHN-treated cells (48 hours). Brightfield shows morphological changes associated with treatment, including cell shrinkage and membrane blebbing. DCF-DA detects ROS levels, indicated by green fluorescence intensity. AO/EtBr Visualizes live (green) and apoptotic/necrotic (orange-red) cells to assess cell death. Images were captured in 20x magnification from Olympus microscope. Data are presented as mean ± SD (n = 3); 95% confidence intervals were calculated for outcome measures.

in cell density and structural integrity. At 24 hours, cells exhibited shrinkage and membrane blebbing, which became more pronounced at 48 hours with detachment and rounding. Fluorescence imaging revealed a progressive increase in intracellular ROS from 24 to 48 hours, accompanied by a shift from viable cells in the control group to early apoptotic cells at 24 hours and late apoptotic/necrotic cells at 48 hours. Notably, the increases in ROS generation and lipid peroxidation remained statistically significant within their respective 95% confidence intervals, confirming the consistency, precision, and reproducibility of the observed oxidative damage. These findings indicate that IHN exerts cytotoxic effects in HepG2 cells through ROS-mediated apoptotic cell death.

Flow cytometry analysis- Cell cycle analysis

As depicted in Figure 3, Flow cytometry of PI-stained HepG2 cells demonstrated that IHN treatment induced a time-dependent G0/G1 cell cycle arrest. In control cells, 52.08% were in G0/G1, 33.71% in S, and 14.08% in G2/M. After 24 hours of IHN exposure, G0/G1 phase cells increased to 74.13%, with a corresponding decline in S (18.86%) and G2/M (6.68%) populations. At 48 hours, this effect was more pronounced, with 83.30% of cells arrested in G0/G1 and further decreases in S (12.05%) and G2/M (4.27%). These results confirm that IHN effectively blocks HepG2 cell cycle progression at the G0/G1 phase.

Apoptosis analysis

As depicted in Figure 4, The apoptotic effect of IHN was further validated using Annexin V-FITC/PI dual staining. Flow cytometry results demonstrated a clear shift in cell populations towards apoptosis following treatment. In the control group, 88.73% of cells were viable (Q1-LL), with only 10.61% undergoing early apoptosis (Q1-LR), and negligible populations in late apoptosis (0.56%, Q1-UR) and necrosis (0.10%, Q1-UL). Upon 24 h treatment with IHN, early apoptotic cells increased to 14.51% and late apoptotic cells to 4.97%, while viable cells decreased to 68.89%. Necrotic cells also increased to 11.63%, suggesting initiation of cell death processes. At 48 h, the pro-apoptotic effect was more pronounced. Early apoptotic cells further increased to 16.00%, and late apoptotic cells reached 5.17%. Necrotic cells were 20.17%, and viable cells reduced significantly to 58.66%. The results collectively indicate that IHN triggers time-dependent apoptosis in HepG2 cells, highlighting its potential as an anti-cancer agent. Together, these findings demonstrate that IHN exerts potent anti-proliferative effects in HepG2 liver cancer cells through induction of G0/G1 cell cycle arrest and promotion of apoptosis in a time-dependent manner. Flow cytometry-based analysis confirms that IHN alters cell cycle dynamics and significantly increases apoptotic cell populations, suggesting its therapeutic promise against HCC.

Metabolic assays- Glucose uptake assay

The glucose uptake assay demonstrated a significant, time-dependent decrease in 2DG levels in HepG2 cells upon treatment with IHN. As shown in Figure 5, untreated control cells exhibited a 2DG uptake level of approximately 66.3 ± 2.5 pmol. Treatment with IHN for 24 hours significantly reduced glucose uptake to 47.8 ± 1.8 pmol ($p < 0.001$), while a further reduction to 41.6 ± 1.9 pmol ($p < 0.001$) was observed at 48 hours. These results indicate that IHN inhibits glycolytic flux by suppressing glucose uptake in HepG2 cells. Similarly, the LDH-A activity assay revealed a marked suppression of enzymatic activity upon IHN treatment. Control HepG2 cells showed LDH-A activity of 6.25 ± 0.3 AU, which decreased significantly to 4.33 ± 0.2 AU ($p <0.01$) after 24 hours of IHN exposure (Figure 5, right panel). At 48 hours, LDH-A activity was further reduced to 3.66 ± 0.2 AU ($p <0.001$). The narrow 95% confidence intervals associated with these reductions confirm the precision, reproducibility, and robustness of the observed metabolic suppression, providing strong mechanistic evidence for the anticancer potential of IHN through metabolic reprogramming.

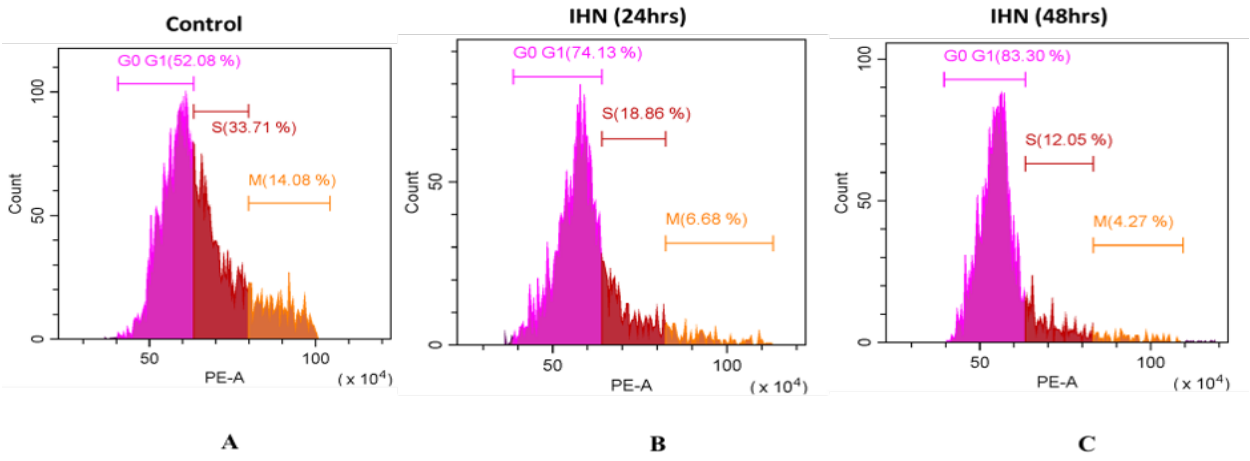

Figure 3. Cell Cycle Analysis of HepG2 Cells Following IHN Treatment. Flow cytometry histograms showing the distribution of HepG2 cells in different cell cycle phases after (A) Control (untreated), (B) 24-hour IHN treatment, and (C) 48-hour IHN treatment. Percentages indicate the proportion of cells in G0/G1 (52.08% control, 74.13% 24h, 83.30% 48h), S, and G2/M phases (14.08% control, 6.68% 24h, 4.27% 48h). The results demonstrate IHN-induced G0/G1 phase arrest in a time-dependent manner (PE-A channel).

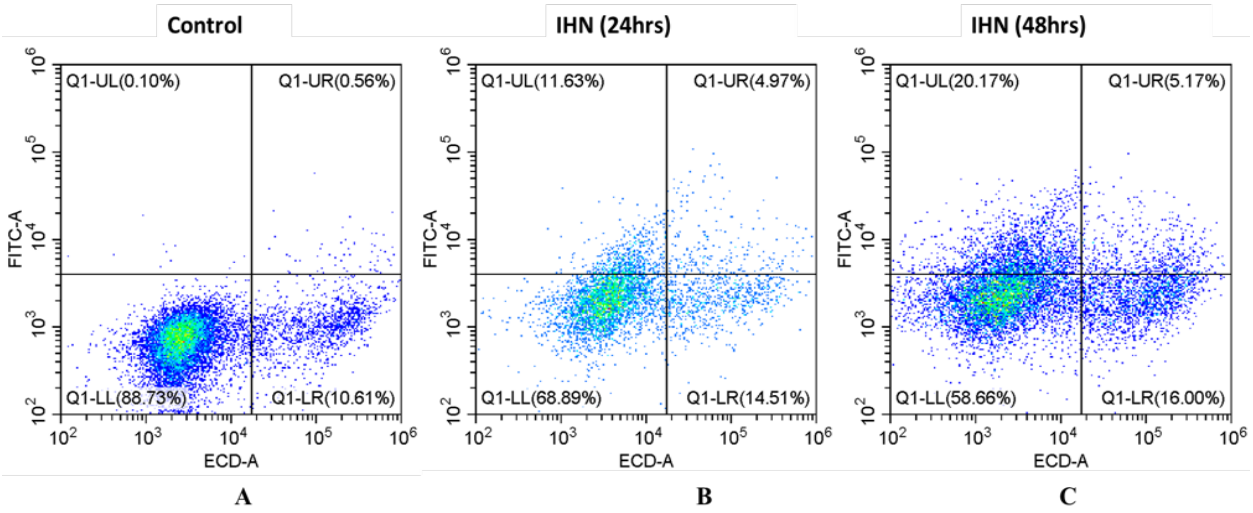

Figure 4. Apoptosis Analysis by Annexin V-FITC/PI Staining. Dot plots showing: (A) Control cells with minimal apoptosis (Q1-UL: 0.10%, Q1-UR: 0.56%), (B) 24-hour, and (C) 48-hour IHN-treated cells. The right upper quadrant (Q1-UR) represents late apoptotic/necrotic cells, showing increased percentages with treatment duration (FITC-A vs. PI channels).

IHN Increases Intracellular oxidative damage in HepG2 Cells

As depicted in Figure 6, exposure to IHN significantly induced oxidative stress in HepG2 cells in a time-dependent manner. Intracellular ROS levels in control cells were maintained at basal levels, whereas treatment with IHN led to a marked increase, showing significant elevation at 24 hours ($p < 0.01$) and further enhancement at 48 hours ($p < 0.001$). Consistent with this, LPO, measured as MDA content, was significantly elevated following IHN treatment; control cells exhibited basal MDA levels of ~2.5 ± 0.2 nmol/mg protein, which increased to ~4.2 ± 0.3 nmol/mg protein at 24 hours ($p < 0.01$) and ~5.1 ± 0.3 nmol/mg protein at 48 hours ($p < 0.001$). These results indicate that IHN promotes both ROS generation and membrane lipid damage, suggesting that the enhanced oxidative burden contributes to cellular damage, apoptosis, and reduced cell viability, thereby highlighting oxidative mechanisms as a key component of its anticancer activity in hepatocellular carcinoma cells. The increase in ROS generation and MDA remained significant within their 95% confidence intervals, indicating consistent oxidative damage following IHN treatment.

IHN Reduces Glutathione Levels and Alters Redox Balance in HepG2 Cells

As shown in Figure 7, treatment with IHN significantly decreased intracellular GSH levels and disrupted the cellular redox balance in HepG2 cells. In control cells, GSH content was maintained at approximately 59 ± 2.8 nmol/10^6 cells. Upon treatment with IHN for 24 hours, GSH levels dropped to ~46 ± 2.5 nmol/10^6 cells ($p < 0.01$), and further declined to ~32 ± 2.7 nmol/10^6 cells ($p < 0.01$) at 48 hours, indicating a time-dependent depletion of antioxidant reserves. Similarly, the GSH/GSSG ratio decreased significantly, from 7.8 ± 0.3 in control cells to ~5.3 ± 0.4 ($p < 0.001$) at 24 hours, and further to ~3.8 ± 0.3 ($p < 0.01$) at 48 hours, highlighting a disruption in cellular redox homeostasis. Collectively, these results demonstrate that IHN promotes oxidative stress in HepG2 cells by reducing intracellular GSH levels and impairing the GSH/GSSG balance in a time-dependent manner. Depletion of GSH levels and disruption of the GSH/GSSG ratio were further validated by 95% confidence interval analysis, reflecting a robust alteration in cellular redox balance.

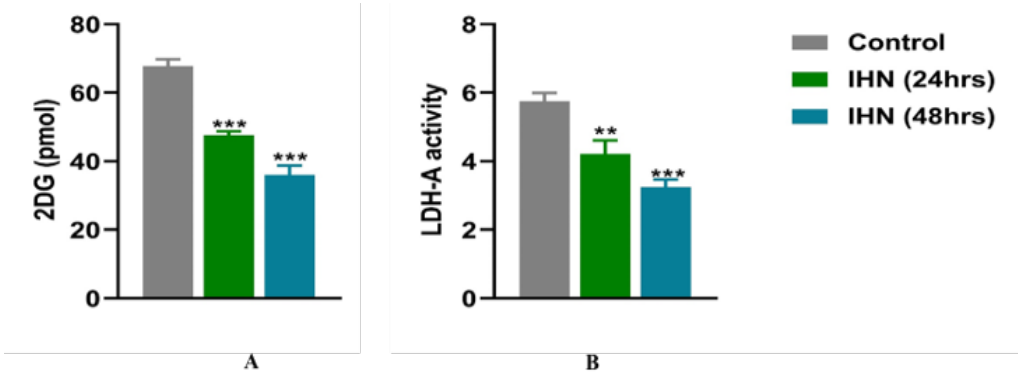

Figure 5. Metabolic Regulation in HepG2 Cells. (A) Glucose uptaken and (B) LDHA activity showing significant decrease after IHN treatment in HepG2 cells. Data represent mean ± SD of three experiments (*p<0.05 vs control). Data are presented as mean ± SD (n = 3); 95% confidence intervals were calculated for outcome measures.

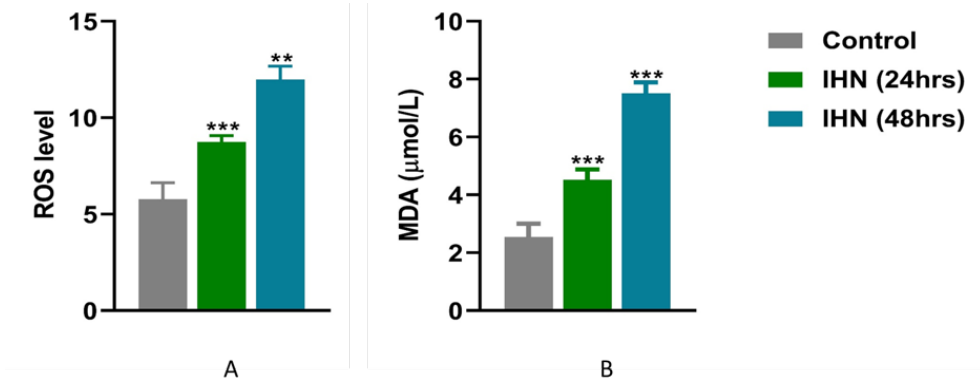

Figure 6. Oxidative Stress Markers in HepG2 Cells

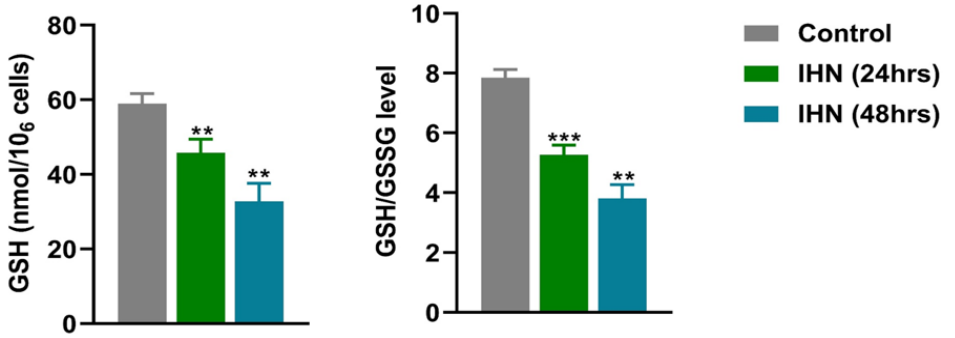

Figure 7. Glutathione Homeostasis Demonstrating GSH Depletion and Altered GSH/GSSG Ratio Following Treatment (control 60, 24hrs : 46, 48hrs : 32 nmol/10^6 cells typographical error). Data represent mean ± SD of three experiments (*p<0.05 vs control). Data are presented as mean ± SD (n = 3); 95% confidence intervals were calculated for outcome measures.

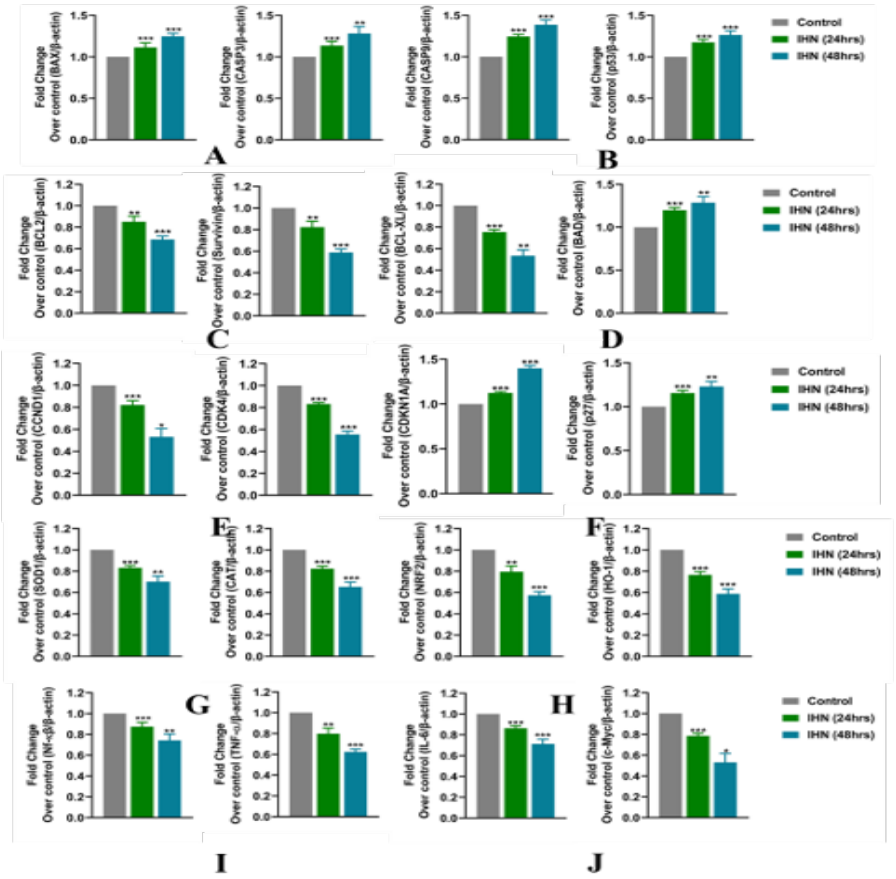

Figure 8. Gene Expressional Analysis by q-RT-PCR in HepG2 Cells. Data are presented as mean ± SD (n = 3); 95% confidence intervals were calculated for key outcome measures.

Gene expression analysis by q-RT-PCR

The RT-PCR analysis revealed significant alterations in the expression of genes associated with apoptosis, cell cycle regulation, and oxidative stress in HepG2 cells following treatment with IHN for 24 and 48 hours (Figure 8). As depicted in Figure 8 (A, B), Exposure to IHN consistently promoted apoptosis and inhibited cell cycle progression in a time-dependent manner, with the effects being more pronounced at 48 hours. This shift toward cell death was driven by a coordinated change in key apoptotic gene families, where pro-apoptotic genes, including BAX, CASP3, CASP9, and p53 were significantly upregulated (up to ≈1.5-fold), while as given in Figure 8 (C, D) whereas anti-apoptotic BCL2 family members (BCL2, Survivin, BCL-XL BAD) were simultaneously downregulated (as low as ≈0.7-fold). Further analysis supported a G1/S phase cell cycle arrest, evidenced by the downregulation of promoters CCND1 and CDK4 and the significant upregulation of inhibitors CDKN1A (p21) and p27 as given in Figure 8 (E, F). Overall, these results demonstrate that IHN induces a strong apoptotic response and inhibits cell growth, which is supported by the decreased expression of proliferation markers like. Concurrent with these changes, IHN exposure resulted in a widespread suppression of the cell's antioxidant defense system, with all analyzed antioxidant genes significantly downregulated as given in Figure (8G, H) stating SOD1 decreased to ≈0.8-fold, CAT dropped to ≈0.65-fold, and the master regulator Nuclear factor erythroid 2-related factor 2 (NRF2) and its target Heme Oxygenase-1 (HO-1) decreased progressively, with HO-1 reaching ≈0.6-fold at 48 hours. Further, it also resulted in a significant and time-dependent suppression of both inflammatory and proliferative gene expression. All tested genes showed progressive downregulation compared to the Control, with the most severe effects observed at 48 hours. Specifically, key inflammatory mediators NF-κβ, TNF-α, and IL-6 were all significantly decreased, with TNF-α showing a substantial reduction to app. 0.63-fold at 48 hours. Concurrent with this suppression of inflammation, the oncogene and proliferation marker c-Myc showed the most drastic downregulation in this group, dropping to approximately ≈0.53-fold at 48 hours as given in Figure (8I, J). The assessment of inflammatory mediator expression highlights that IHN not only induces oxidative and metabolic stress but also suppresses tumor-promoting inflammatory signaling, contributing to its multi-target anticancer effects. Collectively, these results demonstrate that IHN induces a strong apoptotic response, enforces cell cycle arrest, suppresses antioxidant defenses, and inhibits inflammatory and proliferative signaling in HepG2 cells. Importantly, all key gene expression changes were consistent within their respective 95% confidence intervals, underscoring the robustness, reproducibility, and reliability of IHN-mediated modulation of apoptotic, metabolic, antioxidant, and inflammatory signaling pathways.

Effects of isorhamnetin-3-O-neohespeidoside on the mRNA expression of apoptotic (Bax, Caspas-3, Caspase-9 and p53, Bcl2, Bcl-xL, Survivin, Bad) signalling molecules, Cell cycle regulatory molecules (CCND1, CDK4, CDKNIA, p27), antioxidant signalling molecules (SOD, CAT, NRF2, HO-1) and inflammatory signalling (NFKB, TNF-α, IL-1β, C-myc) molecules in HepG2 cells. Cells were treated with isorhamnetin-3-O-neohespeidoside, total RNA was immediately extracted and converted to cDNA. The mRNA expressions were analyzed by real-time PCR using SYBR Green dye. β-Actin was used as an internal control. Target gene expression is normalized to β-Actin mRNA expression and the results are expressed as fold change from control (B). Data represent mean ± SD of three experiments (*$p<0.05$ vs control).

Discussion

The present study demonstrates that IHN exerts strong anti-proliferative and cytotoxic effects against HepG2 hepatocellular carcinoma cells through a coordinated, multi-target mechanism involving early cell-cycle arrest, metabolic inhibition, oxidative stress induction, and activation of intrinsic apoptosis. Rather than acting through a single signaling node, IHN disrupts interconnected regulatory pathways that collectively compromise cancer cell survival. IHN exposure resulted in a clear time-dependent loss of cell viability, reflected by a marked reduction in IC_{50} values from 161.22 μM at 24 h to 95.87 μM at 48 h (Figure 1), indicating increasing cytotoxic potency with prolonged exposure. This effect was accompanied by pronounced morphological alterations, including cell shrinkage, membrane blebbing, and detachment (Figure 2), consistent with stress-induced growth arrest and apoptotic commitment. Flow-cytometric analysis revealed that growth inhibition initially occurred through a robust G0/G1 phase arrest, with cell accumulation rising from 52.08% in controls to 83.30% at 48 h (Figure 3). Molecular analysis confirmed this arrest to be CDKN1A/p21-dependent, driven by suppression of CCND1 and CDK4/6 and upregulation of p21 and p27 (Figure 8E, F), establishing cell-cycle blockade as an early and critical event in IHN action.

Upon prolonged exposure, growth arrest transitioned into apoptotic cell death. Annexin V-FITC/PI staining demonstrated a progressive increase in early and late apoptotic populations, together with necrotic cells at 48 h (Figure 4). This was mechanistically supported by transcriptional activation of the intrinsic mitochondrial apoptotic pathway, evidenced by upregulation of BAX, CASP9, CASP3, and p53, alongside downregulation of anti-apoptotic BCL-2 family members and Survivin (Figure 8A-D). These findings indicate that IHN-induced apoptosis is mitochondria-driven rather than death-receptor-mediated. A central feature of IHN cytotoxicity was the disruption of cellular metabolism and redox homeostasis. Consistent with cancer cells' reliance on aerobic glycolysis, IHN significantly suppressed glycolytic flux by reducing glucose uptake and inhibiting LDH-A activity (from 6.25 ± 0.3 AU to 3.66 ± 0.2 AU at 48 h; Figure 5), indicating effective targeting of the Warburg effect. This metabolic inhibition was closely linked to a pronounced increase in intracellular ROS levels and lipid peroxidation (Figures 2 and 6), suggesting that energy

deprivation sensitizes cells to oxidative injury.

Importantly, IHN not only increased ROS generation but also impaired antioxidant defense capacity. Intracellular GSH levels and the GSH/GSSG ratio declined markedly over time (Figure 7), confirming a collapse in redox buffering capacity. At the molecular level, this imbalance was reinforced by downregulation of NRF2 and its downstream antioxidant targets SOD1, CAT, and HO-1 (Figure 8G, H), indicating that IHN suppresses compensatory antioxidant signaling rather than triggering adaptive cytoprotection. This ROS-NRF2 axis disruption appears to be a pivotal driver of irreversible oxidative damage and apoptotic progression. When compared with previous studies on isorhamnetin (IH), particularly in gastric cancer models where apoptosis was linked primarily to PPAR-γ activation [7], the present findings highlight a mechanistic divergence. While both IH and IHN exert antiproliferative effects at micromolar concentrations, IHN in HepG2 cells predominantly targets redox regulation and metabolic vulnerability. The neohesperidoside moiety may influence cellular uptake, stability, or subcellular targeting, thereby amplifying oxidative stress and metabolic collapse independent of PPAR-γ signaling. Taken together, these findings indicate that IHN-induced reduction in HepG2 cell viability occurs through a sequential and interconnected mechanism, wherein early G0/G1 phase cell-cycle arrest suppresses proliferation, followed by progressive ROS accumulation, lipid peroxidation, and subsequent activation of the intrinsic mitochondrial apoptotic pathway upon prolonged exposure. Based on integrated biochemical, flow cytometric, metabolic, and gene expression analyses, IHN primarily targets the ROS-mediated redox signaling axis, leading to suppression of NRF2-dependent antioxidant defense, activation of the intrinsic mitochondrial apoptotic pathway (BAX, CASP-9, CASP-3), inhibition of glycolytic metabolism (Warburg effect), and induction of G0/G1 cell-cycle arrest via the CDKN1A/p21 pathway.

The major strength of this study lies in its integrative approach, combining cytotoxic, cell-cycle, apoptotic, metabolic, oxidative, and gene-expression analyses to define a coherent mechanistic framework. Nevertheless, limitations include reliance on a single in vitro cancer model and the absence of protein-level and in vivo validation. Future studies should focus on confirming these pathways at the proteomic level, identifying direct molecular targets of IHN, and evaluating therapeutic efficacy and safety in animal models of hepatocellular carcinoma. Exploring combination strategies that exploit redox and metabolic vulnerabilities may further enhance the translational potential of IHN.

In conclusion, the current investigation strongly supports that IHN is a potent cytotoxic agent against HepG2 cells, with an IC50 dropping sharply from 161.22 μM to 95.87 μM at 48 h. Its anti-proliferative effect is mediated by the induction of G0/G1 cell cycle arrest and intrinsic apoptosis. Critically, the primary mechanism drives metabolic catastrophe by suppressing the Warburg effect (LDH-A inhibition). This is coupled with overwhelming pro-oxidant activity, evidenced by high ROS and a collapsed GSH/GSSG redox balance due to paradoxical antioxidant gene downregulation (NRF2). These multi-target findings provide strong evidence for IHN as a therapeutic candidate for hepatocellular carcinoma, warranting further mechanism-focused research on its unique glucoside moiety.

Author Contribution Statement

F. Sherin Rebecca-Preparation of methodology, experimentation, manuscript writing. Rajamanickam Pon Nivedha-Conceptualization sharing, manuscript correction. R.Sharmila, Manuscript review and corrections.

Acknowledgements

None.

Conflict of interest

Nil.

References

1. Oh JH, Jun DW. The latest global burden of liver cancer: A past and present threat. Clin Mol Hepatol. 2023;29(2):355-7. https://doi.org/10.3350/cmh.2023.0070.
2. Kinsey E, Lee HM. Management of hepatocellular carcinoma in 2024: The multidisciplinary paradigm in an evolving treatment landscape. Cancers (Basel). 2024;16(3). https://doi.org/10.3390/cancers16030666.
3. Cragg GM, Pezzuto JM. Natural products as a vital source for the discovery of cancer chemotherapeutic and chemopreventive agents. Med Princ Pract. 2016;25 Suppl 2(Suppl 2):41-59. https://doi.org/10.1159/000443404.
4. Asensi M, Ortega A, Mena S, Feddi F, Estrela JM. Natural polyphenols in cancer therapy. Crit Rev Clin Lab Sci. 2011;48(5-6):197-216. https://doi.org/10.3109/10408363.2011.631268.
5. Cushnie TP, Lamb AJ. Recent advances in understanding the antibacterial properties of flavonoids. Int J Antimicrob Agents. 2011;38(2):99-107. https://doi.org/10.1016/j.ijantimicag.2011.02.014.
6. Shi C, Fan LY, Cai Z, Liu YY, Yang CL. Cellular stress response in eca-109 cells inhibits apoptosis during early exposure to isorhamnetin. Neoplasma. 2012;59(4):361-9. https://doi.org/10.4149/neo_2012_047.
7. Ramachandran L, Manu KA, Shanmugam MK, Li F, Siveen KS, Vali S, et al. Isorhamnetin inhibits proliferation and invasion and induces apoptosis through the modulation of peroxisome proliferator-activated receptor γ activation pathway in gastric cancer. J Biol Chem. 2012;287(45):38028-40. https://doi.org/10.1074/jbc.M112.388702.
8. Boubaker J, Ben Sghaier M, Skandrani I, Ghedira K, Chekir-Ghedira L. Isorhamnetin 3-o-robinobioside from nitraria retusa leaves enhance antioxidant and antigenotoxic activity in human chronic myelogenous leukemia cell line k562. BMC Complement Altern Med. 2012;12:135. https://doi.org/10.1186/1472-6882-12-135.
9. Kim JE, Lee DE, Lee KW, Son JE, Seo SK, Li J, et al. Isorhamnetin suppresses skin cancer through direct inhibition of mek1 and PI3-K. Cancer Prev Res (Phila). 2011;4(4):582-91. https://doi.org/10.1158/1940-6207.Capr-11-0032.
10. Jaramillo S, Lopez S, Varela LM, Rodriguez-Arcos R, Jimenez A, Abia R, et al. The flavonol isorhamnetin exhibits cytotoxic effects on human colon cancer cells. J Agric Food

Chem. 2010;58(20):10869-75. https://doi.org/10.1021/jf102669p.
11. Rana JN, Gul K, Mumtaz S. Isorhamnetin: Reviewing recent developments in anticancer mechanisms and nanoformulation-driven delivery. Int J Mol Sci. 2025;26(15). https://doi.org/10.3390/ijms26157381.
12. Sanchez-Vega F, Mina M, Armenia J, Chatila WK, Luna A, La KC, et al. Oncogenic signaling pathways in the cancer genome atlas. Cell. 2018;173(2):321-37.e10. https://doi.org/10.1016/j.cell.2018.03.035.
13. Park C, Cha HJ, Choi EO, Lee H, Hwang-Bo H, Ji SY, et al. Isorhamnetin induces cell cycle arrest and apoptosis via reactive oxygen species-mediated amp-activated protein kinase signaling pathway activation in human bladder cancer cells. Cancers (Basel). 2019;11(10). https://doi.org/10.3390/cancers11101494.
14. Jayaraman S, Natarajan SR, Veeraraghavan VP, Jasmine S. Unveiling the anti-cancer mechanisms of calotropin: Insights into cell growth inhibition, cell cycle arrest, and metabolic regulation in human oral squamous carcinoma cells (hsc-3). J Oral Biol Craniofac Res. 2023;13(6):704-13. https://doi.org/10.1016/j.jobcr.2023.09.002.
15. Gatasheh MK, Natarajan SR, Krishnamoorthy R, Alsulami TS, Rajagopal P, Palanisamy CP, et al. Molecular analysis to identify novel potential biomarkers as drug targets in colorectal cancer therapy: An integrated bioinformatics analysis. Mol Cell Oncol. 2024;11(1):2326699. https://doi.org/10.1080/23723556.2024.2326699.
16. Natarajan SR, Krishnamoorthy R, Alshuniaber MA, Alsulami TS, Gatasheh MK, Rajagopal P, et al. Abce1 facilitates tumour progression via aerobic glycolysis and inhibits cell death in human colorectal cancer cells through the p53 signalling pathway. Sci Rep. 2025;15(1):24674. https://doi.org/10.1038/s41598-025-92436-4.
17. Prasad M, Gatasheh MK, Alshuniaber MA, Krishnamoorthy R, Rajagopal P, Krishnamoorthy K, et al. Impact of glyphosate on the development of insulin resistance in experimental diabetic rats: Role of nfκb signalling pathways. Antioxidants (Basel). 2022;11(12). https://doi.org/10.3390/antiox11122436.
18. Chen S, Zhao S, Wang X, Zhang L, Jiang E, Gu Y, et al. Crocin inhibits cell proliferation and enhances cisplatin and pemetrexed chemosensitivity in lung cancer cells. Transl Lung Cancer Res. 2015;4(6):775-83. https://doi.org/10.3978/j.issn.2218-6751.2015.11.03.
19. Yan X, Feng C, Chen Q, Li W, Wang H, Lv L, et al. Effects of sodium fluoride treatment in vitro on cell proliferation, apoptosis and caspase-3 and caspase-9 mrna expression by neonatal rat osteoblasts. Arch Toxicol. 2009;83(5):451-8. https://doi.org/10.1007/s00204-008-0365-z.
20. Chen XQ, Yang S, Kang MQ, Li ZY, Lu HS, Lin TY. Survivin expression in human lung cancer and the influence of its downregulation on the biological behavior of human lung cancer cells. Exp Ther Med. 2012;3(6):1010-4. https://doi.org/10.3892/etm.2012.525.
21. Schulze-Bergkamen H, Ehrenberg R, Hickmann L, Vick B, Urbanik T, Schimanski CC, et al. Bcl-x(l) and myeloid cell leukaemia-1 contribute to apoptosis resistance of colorectal cancer cells. World J Gastroenterol. 2008;14(24):3829-40. https://doi.org/10.3748/wjg.14.3829.
22. Nasim B, Mehdi M, Soraya, Marefat, Ardalan M, Mir Davood O. Decreased expression of proapoptotic genes caspase-8- and bcl2-associated agonist of cell death (bad) in ovarian cancer. Clinical Ovarian and Other Gynecologic Cancer. 2014;7(1):18-23. https://doi.org/https://doi.org/10.1016/j.cogc.2014.12.004.
23. Sun J, Feng Q, Xu Y, Liu P, Wu Y. Analysis of prognostic value of lactate metabolism-related genes in ovarian cancer based on bioinformatics. J Ovarian Res. 2024;17(1):110. https://doi.org/10.1186/s13048-024-01426-z.
24. Du B, Wang Z, Zhang X, Feng S, Wang G, He J, et al. Microrna-545 suppresses cell proliferation by targeting cyclin d1 and cdk4 in lung cancer cells. PLoS One. 2014;9(2):e88022. https://doi.org/10.1371/journal.pone.0088022.
25. Brown I, Shalli K, McDonald SL, Moir SE, Hutcheon AW, Heys SD, et al. Reduced expression of p27 is a novel mechanism of docetaxel resistance in breast cancer cells. Breast Cancer Res. 2004;6(5):R601-7. https://doi.org/10.1186/bcr918.
26. Bostwick DG, Alexander EE, Singh R, Shan A, Qian J, Santella RM, et al. Antioxidant enzyme expression and reactive oxygen species damage in prostatic intraepithelial neoplasia and cancer. Cancer. 2000;89(1):123-34.
27. Abdelmagid SA, Rickard JA, McDonald WJ, Thomas LN, Too CK. Cat-1-mediated arginine uptake and regulation of nitric oxide synthases for the survival of human breast cancer cell lines. J Cell Biochem. 2011;112(4):1084-92. https://doi.org/10.1002/jcb.23022.
28. Zhang M, Zhang C, Zhang L, Yang Q, Zhou S, Wen Q, et al. Nrf2 is a potential prognostic marker and promotes proliferation and invasion in human hepatocellular carcinoma. BMC Cancer. 2015;15:531. https://doi.org/10.1186/s12885-015-1541-1.
29. Furfaro AL, Piras S, Domenicotti C, Fenoglio D, De Luigi A, Salmona M, et al. Role of nrf2, ho-1 and gsh in neuroblastoma cell resistance to bortezomib. PLoS One. 2016;11(3):e0152465. https://doi.org/10.1371/journal.pone.0152465.
30. Csiszár A, Szentes T, Haraszti B, Balázs A, Petrányi GG, Pócsik E. The pattern of cytokine gene expression in human colorectal carcinoma. Pathol Oncol Res. 2004;10(2):109-16. https://doi.org/10.1007/bf02893465.
31. Taira N, Mimoto R, Kurata M, Yamaguchi T, Kitagawa M, Miki Y, et al. Dyrk2 priming phosphorylation of c-jun and c-myc modulates cell cycle progression in human cancer cells. J Clin Invest. 2012;122(3):859-72. https://doi.org/10.1172/jci60818.